ELECTROMAGNETIC SCATTERING FROM RADIALLY OR AXIALLY INHOMOGENEOUS OBJECTS

Ahmed A. Kishk
Department of Electrical Engineering
University of Mississippi
University MS 38677

Mohamed Abouzahra
Massachusetts Institute of Technology
Lincoln Laboratory
Lexington, MA 02173

ABSTRACT

A computer program based on the method of moments approach is developed to compute electromagnetic scattering from axisymmetric objects. The object may consist of N linear isotropic homogeneous regions. These regions may be arranged axially and/or radially with the axis of symmetry. Surface integral equations (SIE) formulation, E-PMCHW, is used to formulate the problem. Other formulations can easily be incorporated in the computer code. Bistatic and monostatic Radar Cross Sections (RCS) for several benchmark geometries are computed. The computed results are verified by comparison with measured and exact calculated results. In some cases the self-consistency method is used to perform the verification. The measured and calculated data presented in this paper are expected to serve as benchmarks for other researchers in the field.[1]

I INTRODUCTION

The study of electromagnetic scattering from composite materials has become of interest to many engineering societies. For example, in biomedicine modeling of human bodies and tissues requires very complex composite objects. With the relative increase in the complexity of the objects of interest, numerical solutions become necessary to study the electromagnetic characteristics of these objects. Various numerical methods can be used to solve such problems

1 This work was sponsored by the Department of the Air Force. The views expressed are those of the authors and do not reflect the official policy or position of the US Government.

[1-6], however, each method has limitations.

The method of moments has been proven to be efficient in solving Surface Integral Equations (SIE). The SIE formulation is most suitable for objects made of linearly isotropic homogeneous materials. For inhomogeneous objects, other formulations may be used, such as the Volume Integral Equations (VIE) or Partial Differential Equations (PDE) formulations. However, if the inhomogeneity of the material is simple, the use of SIE may be preferred, because the matrix size will be smaller using SIE than the matrices that can be obtained from other formulations.

In this paper, the SIE formulation is used to assess the problem of electromagnetic scattering from bodies of revolution made of multihomogeneous regions. The present formulation is similar to the one given in [1]. The method of moments is used to solve the SIE. The resulting matrix system is a buildup of the basic Z and Y matrix obtained for conducting or dielectric bodies of revolution [7-8]. The computer program that has been developed to compute the bistatic or monostatic Radar Cross Sections (RCS) is tested and verified, and several examples are selected to show the accuracy of this program in predicting RCS. Only one formulation is discussed; however, the program has been written to implement easily other surface formulations, such as those reported in [9]. Also, the program is written to efficiently fill the matrix. The properties of symmetry in reference to the impedance and admittance matrices that are used to build the final matrix are implemented. All the numerical results presented in this paper are obtained by the same program (MRBOR) to show its flexibility and generality.

II DEVELOPMENT OF THE SIE

a. Statement of the Problem:

In this section, the concept of the equivalence principle is used to derive the SIE formulation for composite scatterers with N homogeneous regions. The geometry and notations for such a scatterer are given in Fig. 1. The whole space is divided into N+1 homogeneous regions with permittivities ϵ_i and permeabilities μ_i, i = 0, 1, 2, ..., N. Lossy materials are considered by allowing ϵ_i, μ_i, i = 1, 2, ..., N to be complex. Some homogeneous regions are considered to be perfect conductors. The region V_i is surrounded by a closed surface S_i and recognized by the inward normal unit vector **n**. The surface interface between regions V_i and

V_j is S_{ij}, $i \neq j$. Thus, S_i is the set of all interface surfaces S_{ij}, where j represents all region numbers interfacing with region V_i. Note that S_{ij} is the same surface as S_{ji}; however, the normal unit vectors $\mathbf{n}_i$ and $\mathbf{n}_j$ are in opposite directions to each other on S_{ij}.

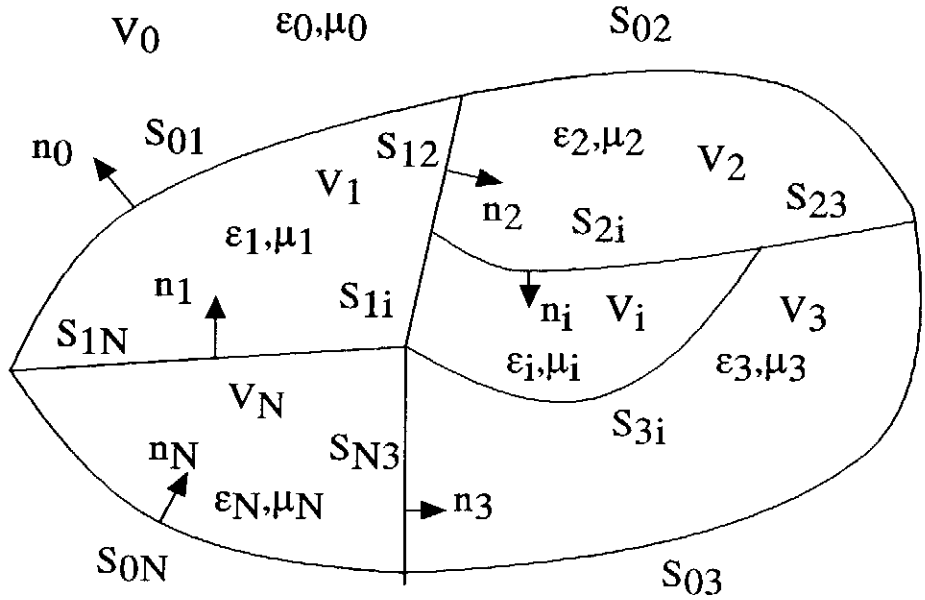

Fig. 1. General geometry of an object consisting of N regions.

b.SIE Formulation:

The total fields in each homogeneous region are denoted by $\mathbf{E}_i$ and $\mathbf{H}_i$, i = 0, 1, 2, ..., N for the electric and magnetic fields, respectively. If V_i is a perfectly conducting region, the fields are equal to zero. In the free-space region V_0, the total fields ($\mathbf{E}_0$, $\mathbf{H}_0$) are the summation of the incident and scattered fields ($\mathbf{E}^{inc} + \mathbf{E}^{sc}$, $\mathbf{H}^{inc} + \mathbf{H}^{sc}$). From Maxwell's equations and the equivalence principle, one can express the field in each region in terms of unknown electric- and magnetic-equivalent surface currents. In this paper, the sources of excitation are considered to be due to a plane wave in the free space region; therefore, the fields at any observation point $\mathbf{r}$ in the free space can be expressed as [1] (these expressions are given here for convenience)

$$\theta(\mathbf{r})\,\mathbf{E}_0(\mathbf{r}) = \mathbf{E}^{inc} - L^0_{S_0}\mathbf{J}_0(\mathbf{r}') + \kappa^0_{S_0}\mathbf{M}_0(\mathbf{r}') \tag{1}$$

$$\theta(\mathbf{r})\,\mathbf{H}_0(\mathbf{r}) = \mathbf{H}^{inc} - \kappa^0_{S_0}\,\mathbf{J}_0(\mathbf{r}') - (1/\eta_0^2)\,L^0_{S_0}\,\mathbf{M}_0(\mathbf{r}') \tag{2}$$

and

$$\theta(\mathbf{r})\ \mathbf{E}_i(\mathbf{r}) = -L^i_{S_i}\ \mathbf{J}_i(\mathbf{r}') + \kappa^i_{S_i}\ \mathbf{M}_i(\mathbf{r}') \tag{3}$$

$$\theta(\mathbf{r})\ \mathbf{H}_i(\mathbf{r}) = -\kappa^i_{S_i}\ \mathbf{J}_i(\mathbf{r}') - (1/\eta_i^2)\, L^i_{S_i}\ \mathbf{M}_i(\mathbf{r}') \tag{4}$$

in the region V_i, where i = 1, 2, ... N. Time variation of $e^{j\omega t}$ is implied and suppressed throughout. The electric- and magnetic-surface currents along the boundaries are

$$\begin{aligned} \mathbf{J}_i &= \mathbf{n}_i \times \mathbf{H}_i \\ \mathbf{M}_i &= -\mathbf{n}_i \times \mathbf{E}_i \end{aligned} \qquad \text{on } S_i \tag{5}$$

In these equations, $\eta_i = \eta_0 \sqrt{\mu_{ir}/\epsilon_{ir}}$, $\epsilon_i = \epsilon_0\ \epsilon_{ir}$, $\mu_i = \mu_0\mu_{ir}$, ϵ_{ir} and μ_{ir} are the relative permittivity and permeability in the region V_i, and η_0 is the intrinsic impedance of the free space. The operators L^i_S and κ^i_S are defined as

$$L^i_{S_i}\mathbf{C}_i(\mathbf{r}') = j\omega\mu_i \int_{S_i} [\mathbf{C}_i(\mathbf{r}') + (1/\omega^2\epsilon_i\mu_i)\ \nabla\nabla'.\mathbf{C}_i(\mathbf{r}')]\,\Phi_i\, dS' \tag{6}$$

$$\kappa^i_{S_i}\ \mathbf{C}_i\ (\mathbf{r}') = \int_{S_i} \mathbf{C}_i\ (\mathbf{r}') \times \nabla\ \Phi_i\ dS' \tag{7}$$

where $\mathbf{C}_i(\mathbf{r}')$ represents the currents $\mathbf{J}_i$ or $\mathbf{M}_i$. For $\mathbf{r} = \mathbf{r}'$, the operators are interpreted as Cauchy principal-value integrals. Φ_i is the Green's function of unbounded region, which can be represented as

$$\Phi_i\ (\mathbf{r} - \mathbf{r}') = e^{-jk_i|\mathbf{r} - \mathbf{r}'|}/|\mathbf{r} - \mathbf{r}'| \tag{8}$$

where k_i is the wave number of the region i, which is equal to $\omega\sqrt{\epsilon_i\mu_i}$. In Equations (1) to (4) the value of $\theta(\mathbf{r})$ is constant, depending on the position of $\mathbf{r}$ as

$$\theta(\mathbf{r}) = \left\{ \begin{array}{c} 1 \text{ for } \mathbf{r} \in V_i \\ 1/2 \text{ for } \mathbf{r} \in S_i \\ 0 \text{ elsewhere} \end{array} \right\} \tag{9}$$

Applying the boundary conditions on each S_{ij} yields a set of coupled integral equations for the unknown electric and magnetic currents on these surfaces. On the dielectric interfaces, the tangential fields are continuous. Thus,

$$\mathbf{E}_i|_{tan} = \mathbf{E}_j|_{tan} \quad \text{on } S_{ij} \tag{10}$$

$$\mathbf{n}_i \times \mathbf{H}_i = \mathbf{n}_i \times \mathbf{H}_j \quad \text{on } S_{ij} \tag{11}$$

On the conductor interfaces, the tangential electric fields vanish, yielding

$$\mathbf{E}_i|_{tan} = \mathbf{0} \quad \text{on } S_{ij} \text{ (conductor surfaces)} \tag{12}$$

Substituting Equations (1) to (4) into (10) to (12), one obtains

$$[L^i_{S_i}\mathbf{J}_i - \kappa^i_{S_i}\mathbf{M}_i - L^j_{S_j}\mathbf{J}_j + \kappa^j_{S_j}\mathbf{M}_j]_{tan} = \begin{Bmatrix} \mathbf{0} \text{ i nor j} = 0 \\ \mathbf{E}^{inc}_{tan} \text{ i or j} = 0 \end{Bmatrix} \quad \text{on } S_{ij} \tag{13}$$

$$\mathbf{n}_i \times [\kappa^i_{S_i}\mathbf{J}_i + (1/\eta_i^2) L^i_{S_i}\mathbf{M}_i] - \mathbf{n}_i \times [\kappa^j_{S_j}\mathbf{J}_j + 1/\eta_j^2 L^j_{S_j}\mathbf{M}_j] = \begin{Bmatrix} \mathbf{0} \text{ i nor j} = 0 \\ \mathbf{n}_i \times \mathbf{H}^{inc} \text{ i or j} = 0 \end{Bmatrix} \quad \text{on } S_{ij} \tag{14}$$

$$[L^i_{S_i}\mathbf{J}_i - \kappa^i_{S_i}\mathbf{M}_i]_{tan} = \begin{Bmatrix} \mathbf{0} \text{ i nor j} = 0 \\ \mathbf{E}^{inc}_{tan} \text{ i or j} = 0 \end{Bmatrix} \quad \text{on } S_{ij} \tag{15}$$

To enable the reader to have better understanding of Equations (13) to (15) (which yield a coupled system of integral equations), a specific example will be considered. Consider a scatterer consisting of two dielectric regions attached to a perfectly conducting body, all in free space, as shown in Fig. 2. The boundary conditions in integral forms are

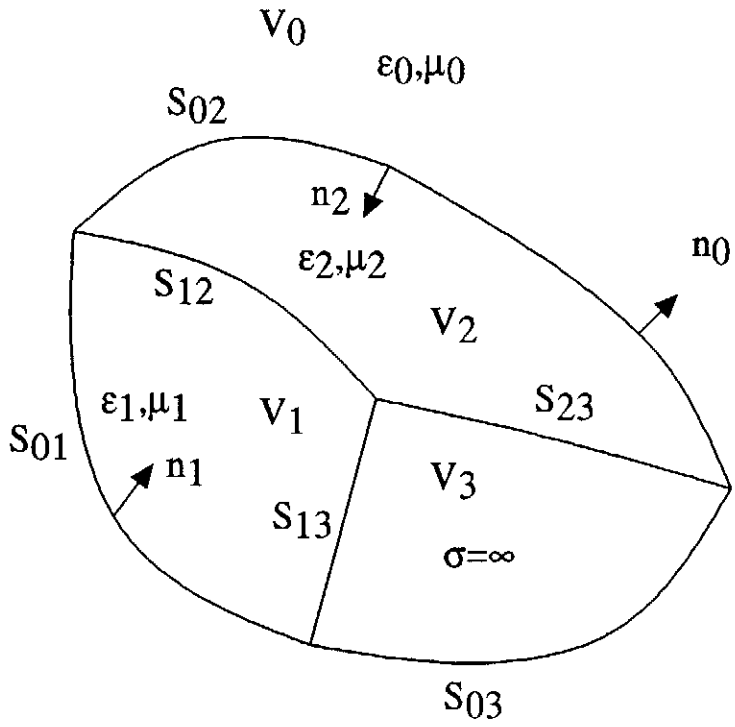

Fig. 2. Example of a three regions object.

$$[L^0_{S_0} \mathbf{J}_0 - \kappa^0_{S_0} \mathbf{M}_0 - L^1_{S_1} \mathbf{J}_1 + \kappa^1_{S_1} \mathbf{M}_1]_{tan} = \mathbf{E}^{inc}_{tan} \quad \text{on } S_{01} \tag{16}$$

$$\begin{aligned} \mathbf{n}_0 \times [\kappa^0_{S_0} \mathbf{J}_0 + (1/\eta_0^2)\, L^0_{S_0} \mathbf{M}_0] - \mathbf{n}_0 \times [\kappa^1_{S_1} \mathbf{J}_1 + (1/\eta_1^2)\, L^1_{S_1} \mathbf{M}_1] \\ = \mathbf{n}_0 \times \mathbf{H}^{inc} \quad \text{on } S_{01} \end{aligned} \tag{17}$$

where

$$\begin{aligned} \mathbf{J}_0 &= (\mathbf{J}_{01}, \mathbf{J}_{02}, \mathbf{J}_{03}) \\ \mathbf{J}_1 &= (-\mathbf{J}_{01}, \mathbf{J}_{12}, \mathbf{J}_{13}) \\ \mathbf{M}_0 &= (\mathbf{M}_{01}, \mathbf{M}_{02}) \\ \mathbf{M}_1 &= (-\mathbf{M}_{01}, \mathbf{M}_{12}) \end{aligned} \tag{18}$$

$$[L^0_{S_0}\,\mathbf{J}_0 - \kappa^0_{S_0}\,\mathbf{M}_0 - L^2_{S_2}\,\mathbf{J}_2 + \kappa^2_{S_2}\,\mathbf{M}_2\,]_{tan} = \mathbf{E}^{inc}_{tan} \quad \text{on } S_{02} \tag{19}$$

$$\begin{aligned}\mathbf{n}_0 \times [\kappa^0_{S_0}\,\mathbf{J}_0 + (1/\eta_0^2)\,L^0_{S_0}\mathbf{M}_0] - \mathbf{n}_0 \times [\kappa^2_{S_2}\mathbf{J}_2 + (1/\eta_2^2)\,L^2_{S_2}\,\mathbf{M}_2] \\ = \mathbf{n}_0 \times \mathbf{H}^{inc} \quad \text{on } S_{02}\end{aligned} \tag{20}$$

where

$$\begin{aligned}\mathbf{J}_2 &= (-\mathbf{J}_{02},\ \mathbf{J}_{12},\ \mathbf{J}_{23}\ ) \\ \mathbf{M}_2 &= (-\mathbf{M}_{02},\ -\mathbf{M}_{12})\end{aligned} \tag{21}$$

$$[L^0_{S_0}\,\mathbf{J}_0 - \kappa^0_{S_0}\,\mathbf{M}_0\,]_{tan} = \mathbf{E}^{inc}_{tan} \quad \text{on } S_{03} \tag{22}$$

$$[L^1_{S_1}\,\mathbf{J}_1 - \kappa^1_{S_1}\,\mathbf{M}_1 - L^2_{S_2}\,\mathbf{J}_2 + \kappa^2_{S_2}\,\mathbf{M}_2\,]_{tan} = \mathbf{E}^{inc}_{tan} \quad \text{on } S_{12} \tag{23}$$

$$\begin{aligned}\mathbf{n}_1 \times [\kappa^1_{S_1}\,\mathbf{J}_1 + (1/\eta_1^2)\,L^1_{S_1}\mathbf{M}_1] - \hat{\mathbf{n}}1 \times [\kappa^2_{S_2}\mathbf{J}_2 + (1/\eta_2^2)\,L^2_{S_2}\,\mathbf{M}_2] \\ = \mathbf{n}_1 \times \mathbf{H}^{inc} \quad \text{on } S_{12}\end{aligned} \tag{24}$$

$$[L^1_{S_1}\,\mathbf{J}_1 - \kappa^1_{S_1}\,\mathbf{M}_1\,]_{tan} = \mathbf{E}^{inc}_{tan} \quad \text{on } S_{13} \tag{25}$$

$$[L^2_{S_2}\,\mathbf{J}_2 - \kappa^2_{S_2}\,\mathbf{M}_2\,]_{tan} = \mathbf{E}^{inc}_{tan} \quad \text{on } S_{23} \tag{26}$$

These are nine vectorial equations in nine vectorial unknowns. The unknowns are the electric- and magnetic-surface currents $\mathbf{J}_{01}$, $\mathbf{J}_{02}$, $\mathbf{J}_{03}$, $\mathbf{J}_{12}$, $\mathbf{J}_{13}$, $\mathbf{J}_{23}$, $\mathbf{M}_{01}$, $\mathbf{M}_{02}$, and $\mathbf{M}_{12}$. The integral equations are reduced to matrix equations using the method of moments by using triangle testing and triangle expansion functions [8].

The above surface integral equations are applied to rotationally-symmetric bodies. The reduction of the integral equations to matrix equations involving unknown surface currents follows a well-known procedure [9]. After the necessary manipulations of the method of moments, the general matrix takes the form

$$[\ T\ ]_n\ [I]_n\ =\ [V]_n \tag{27}$$

where T is a square matrix, representing a combination of impedance and admittance submatrices that are given in [9]; I_n is a column matrix for the unknown expansion coefficients of the unknown current components J and M; and V_n is the excitation column matrix. Once the matrix is solved, the induced currents on all surface interfaces can be determined. Scattered far fields can be determined from the induced currents on the outer surfaces.

III RESULTS AND DISCUSSION

a. Bistatic RCS:

In this section the bistatic RCS is computed numerically. The numerical results are verified by comparison with analytical and supplemental numerical results.

Dielectric sphere: First, to verify the numerical results of objects made of more than one homogeneous region, the example of a sphere geometry is considered. The series solution for a dielectric sphere [10] having ϵ_r= 4-j0.5, μ_r= 2-j0.25, and ka=3 is obtained and compared with the numerical solution of the same object when it is divided into three homogeneous regions of the same material type. The results obtained from both solutions must be identical, because physically both cases represent the same object. The agreement between the two solutions is excellent, as shown in Fig. 3. Several spherical objects have been considered, such as the coated sphere and the multilayered sphere; however, their results have been omitted for brevity.

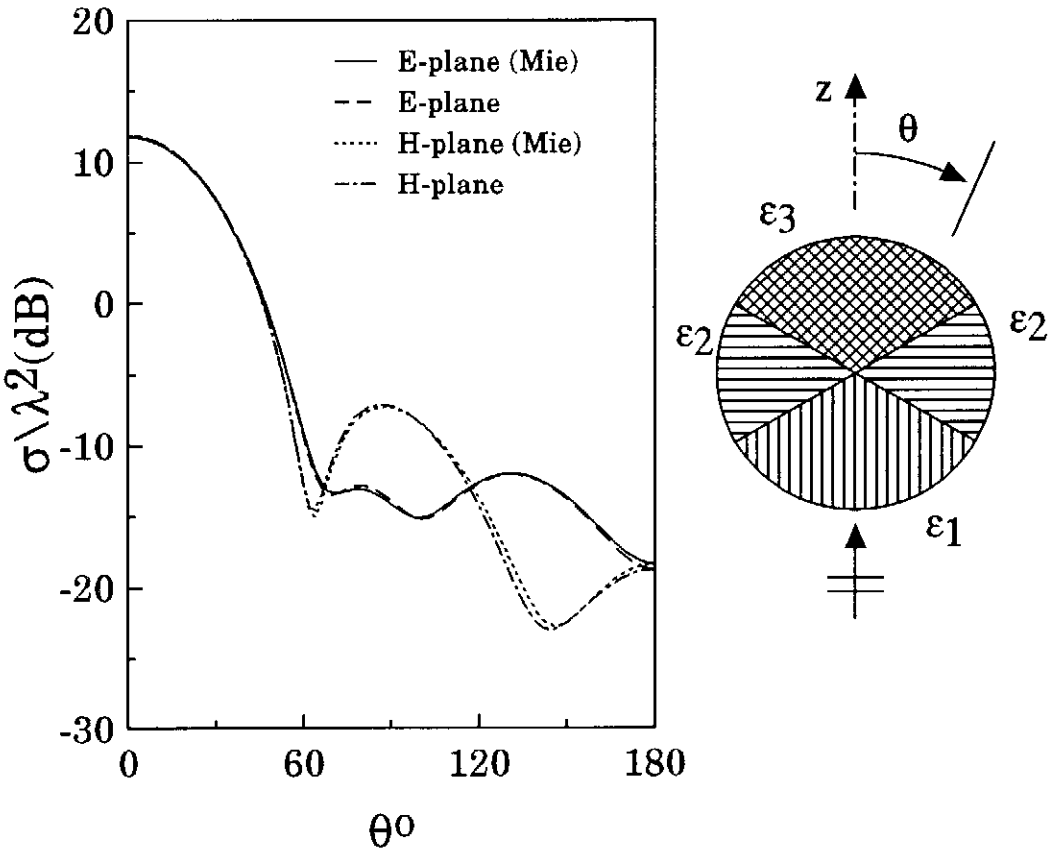

Fig. 3. Bistatic RCS of dielectric sphere divided into three regions of the same materials, ϵ_r=4-j0.5, μ_r=2-j0.25, and ks=3.

Dielectric toroid: Another geometry, of a dielectric toroid, is considered, as shown in Fig.4a. The numerical solution is obtained, once, when the circular cross section is divided into six regions, all of which have the same type of material. This numerical solution is compared with the numerical solution of the same object when it is treated as one region. The agreement between both solutions is excellent, as shown in Fig.4b. When each region is filled with different homogeneous materials, the computed bistatic RCS is shown in Fig. 5. Notice that the scattering level has increased in the whole bistatic range.

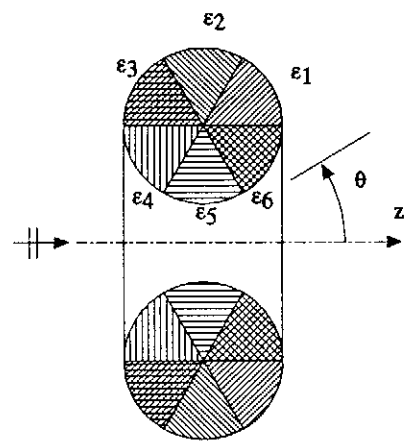

Fig. 4a. Toroid cross section divided into six homogeneous regions.

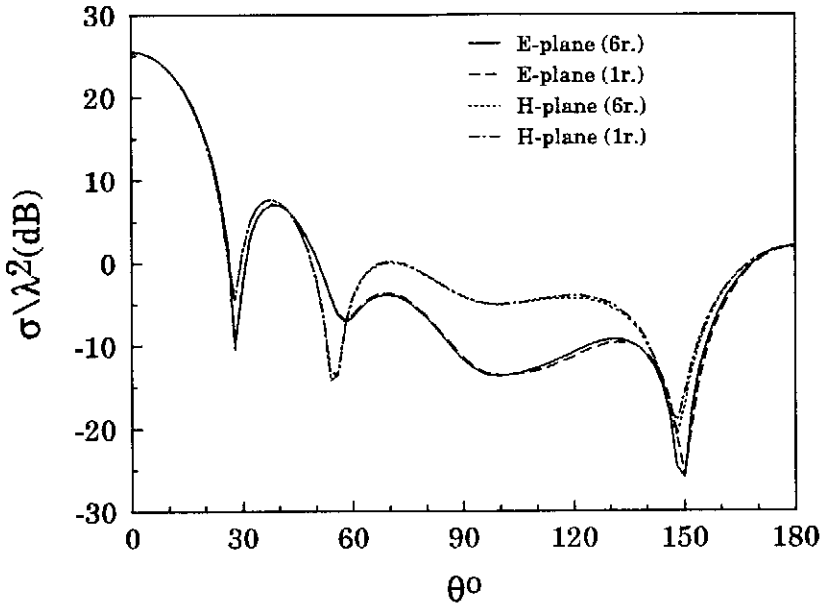

Fig. 4b. Bistatic RCS of the toroid when all regions have the same materials, ϵ_r=4-j0.5, μ_r=2-j0.25, ka=3, kb=4.4.

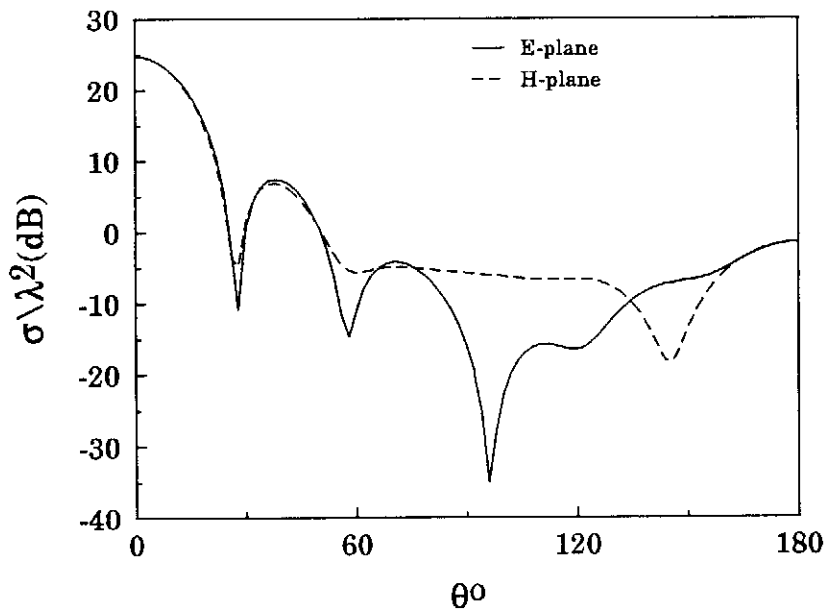

Fig. 5. Bistatic RCS of the toroid with, ϵ_{r1}=3-j3, ϵ_{r2}=2-j2, ϵ_{r3}=4-j0.5, ϵ_{r4}=6-j6, ϵ_{r5}=5-j5, ϵ_{r6}=4-j4, and μ_r=2-j0.25 in all regions.

Loaded conducting bicone: To examine the numerical solution performance of objects made of dielectric and conductors, the case of a biconical conducting object is selected. The numerical solution of this object and the conducting bicone is compared with the numerical solution of a conducting bicone surrounded by an artificial dielectric material of free-space permittivity and permeability, as shown in Fig. 6. In this example, the bicone is illuminated by a plane wave of normal incidence (θ=90°). Therefore, the number of the azimuthal modes that is used to obtain the bistatic RCS is eleven, n=0,..., $\pm$5; for the axial incident cases the required modes are $\pm$1. Figure 6 shows the excellent agreement between the two solutions. Also shown is the symmetry around θ=90°. In this example, the H-plane shows a zero-back and forward-scattering, and the E-plane shows its maximum values at these directions. When the free-space part of this object is filled with homogeneous materials of ϵ_r = 4, the RCS is computed as shown in Fig. 7. The sidelobes of the scattered H-plane patteren disappear, and the forward scattering for the E-plane pattern becomes higher than the back-scattering.

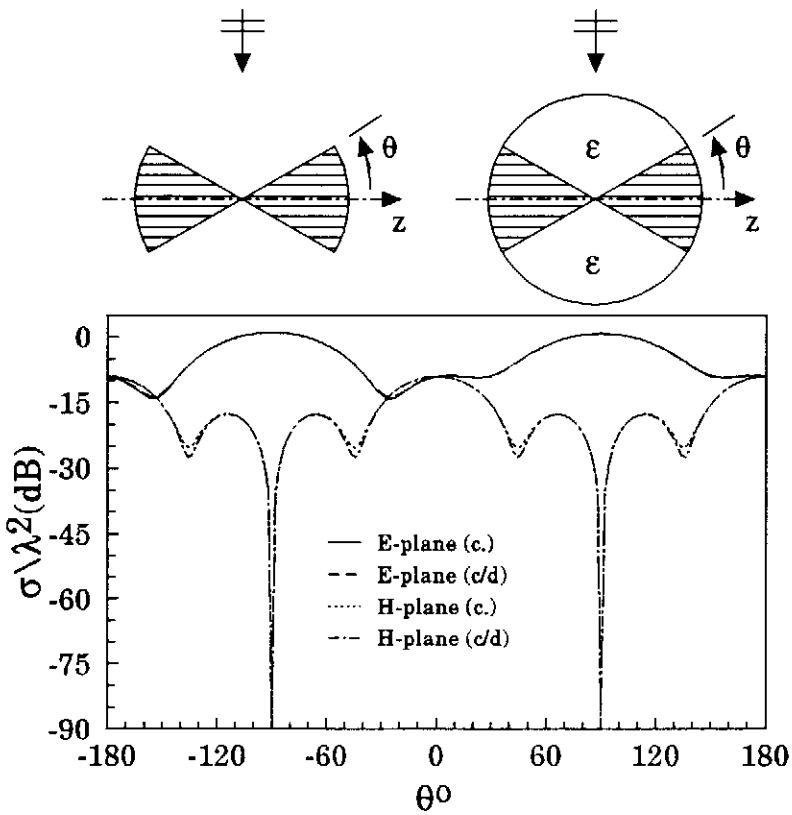

Fig. 6. Bistatic RCS of a conducting bicone, ka=3, ϵ_r=1., μ_r=1.

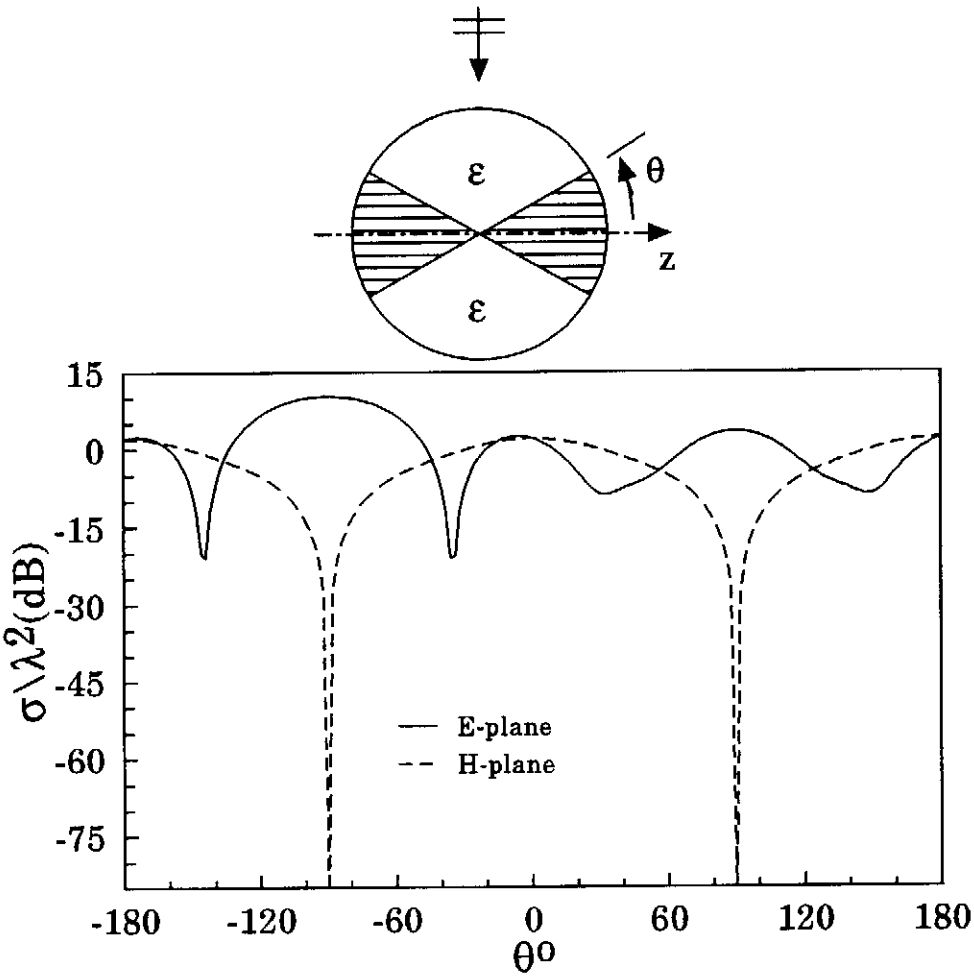

Fig. 7. Bistatic RCS of the bicone when ϵ_r=4., μ_r=1.

b. Monostatic RCS:

In the above examples, the bistatic RCS were considered. Next monostatic RCS are also verified numerically and experimentally.

Half-conducting sphere: The first example is the perfectly-conducting dielectric hemisphere. For numerical verification, the dielectric is considered as a free space. The monostatic RCS is compared with the numerical solution of a conducting hemisphere, as shown in Fig. 8. This figure indicates excellent agreement between both solutions in the whole θ range. When the free-space part is replaced by materials of ϵ_r=2-j0.5, and μ_r=3-j0.5, the monostatic RCS is computed as shown in Fig. 9. The effect of the presence of dielectric materials

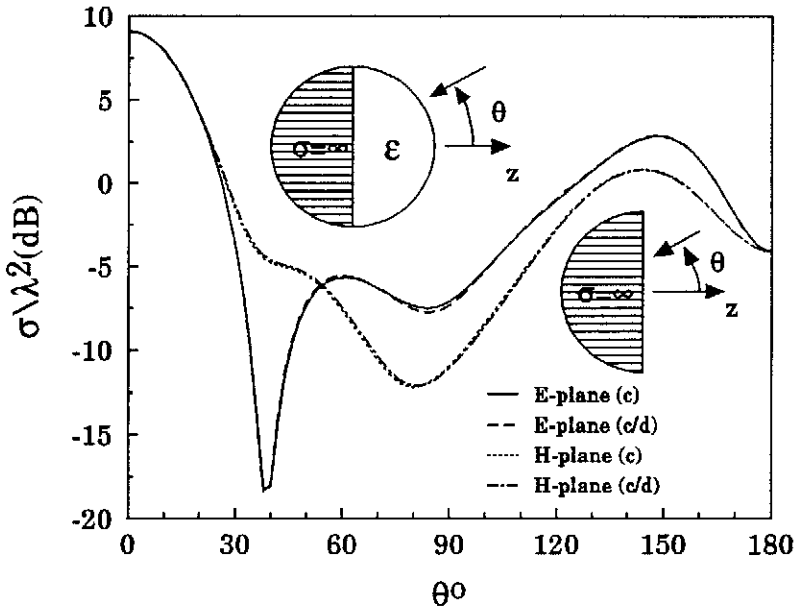

Fig. 8. Monostatic RCS of a conducting hemisphere compared with the scattering from a conducting hemisphere-air hemisphere object, ka=3.

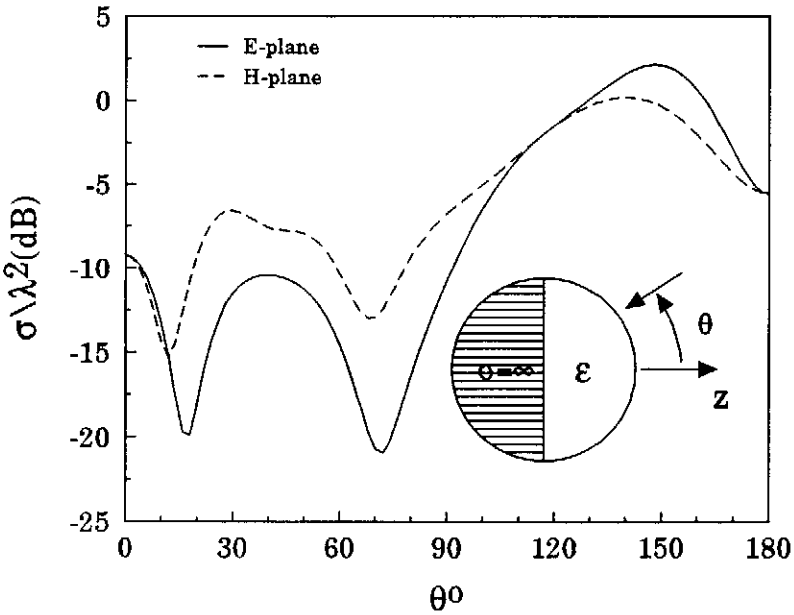

Fig. 9. Monostatic RCS of a conducting hemisphere-dielectric hemisphere object, ka=3, ϵ_r=2-j0.5, μ_r=3-j0.5.

is different from the free space. This difference is clear in the backscattering data for ranges of $\theta<90$, which is the dielectric side. Significant reduction of the backscattering level is observed. When $\epsilon_r=1$, the effect of the flat surface and the sharp edges obviously contributed to the high backscattering levels.

Round-tip cone: In this section, new numerical results are presented and verified with measurements, which have been collected at the RCS Range of Group 95 at Lincoln Laboratory. The first geometry that is considered is the partially coated, perfectly conducting round-tip cone, shown in Fig. 10. The first case that has been considered is the one that corresponds to a homogeneous coating; in other words, the materials in both coating regions are the same. The monostatic RCS are shown in Fig. 11 for both $\theta\theta$ polarization (left) and $\phi\phi$ polarization (right), respectively. When the coating on the second region is removed, the second region is then equivalent to free-space permittivity. The monostatic RCS is computed and compared with the measurements as shown in Fig. 12 for $\theta\theta$ polarization and $\phi\phi$ polarization, respectively. Figure 13 show the monostatic RCS of both polarizations when second region is filled with materials of $\epsilon_r=2.60$. In the above three cases, excellent agreement is obtained between the measured data and the computed data.

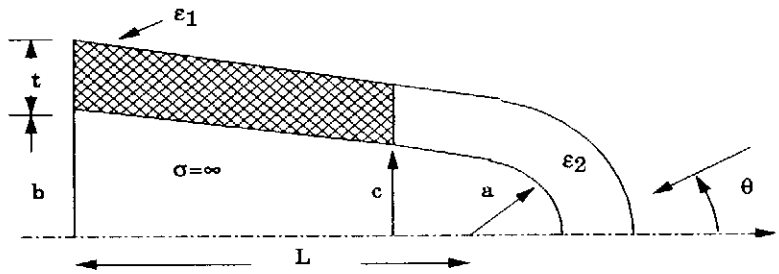

All dimensions in λ_0 (free space wavelength)

L = 1.978, b = 0.2328, a = 0.0424, t = 0.0847 c = 0.86

case	ε_{r1}	ε_{r2}
1	2.05	2.05
2	2.05	1.00
3	2.05	2.60

Fig. 10. Geometry of a partially coated, perfectly conducting round-tip cone.

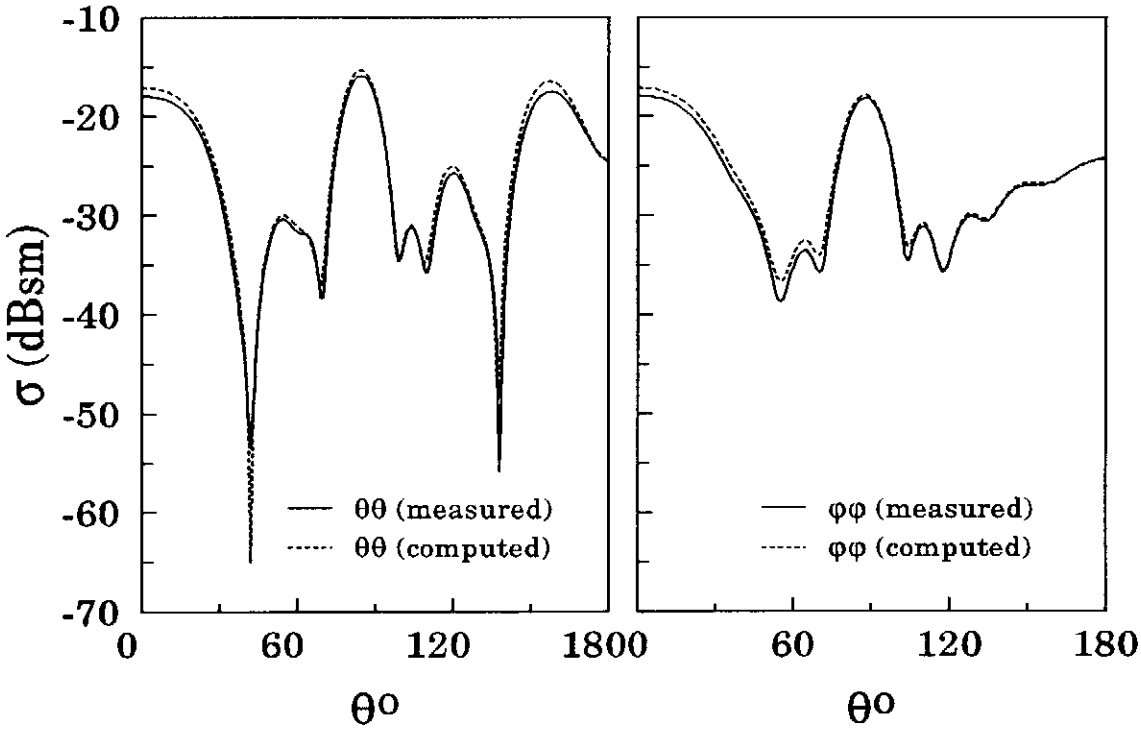

Fig. 11. Computed and measured monostatic RCS of case1 in Fig. 10.

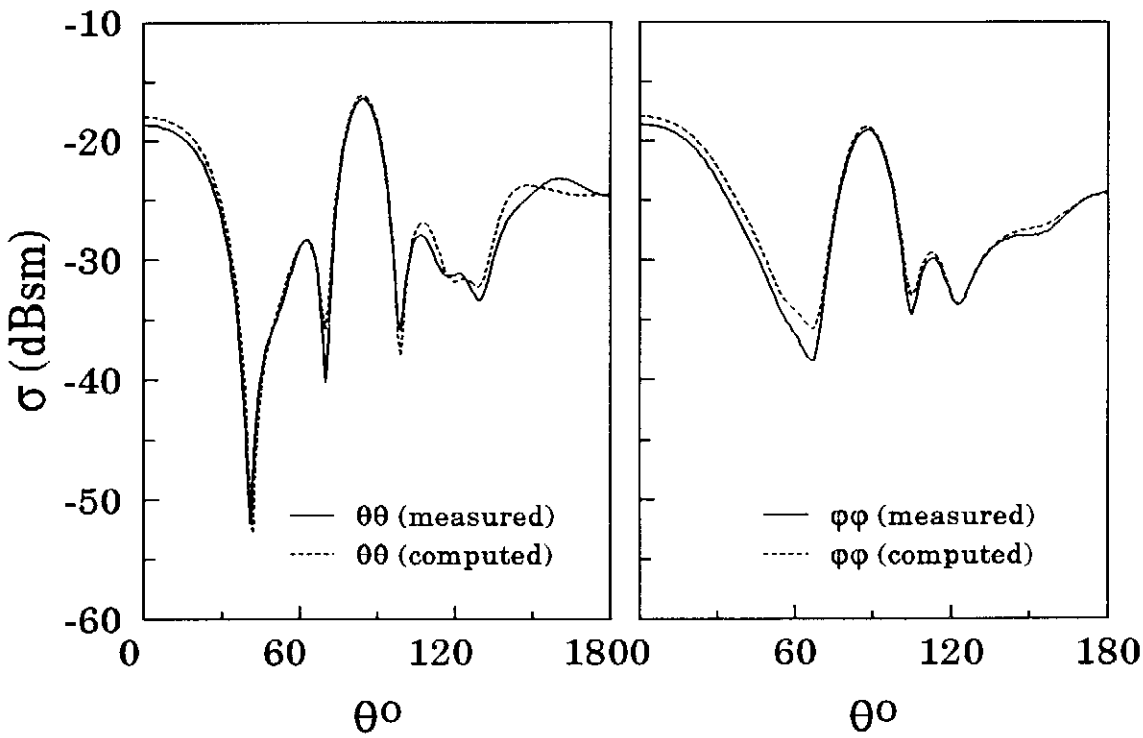

Fig. 12. Computed and measured monostatic RCS of case2 in Fig. 10.

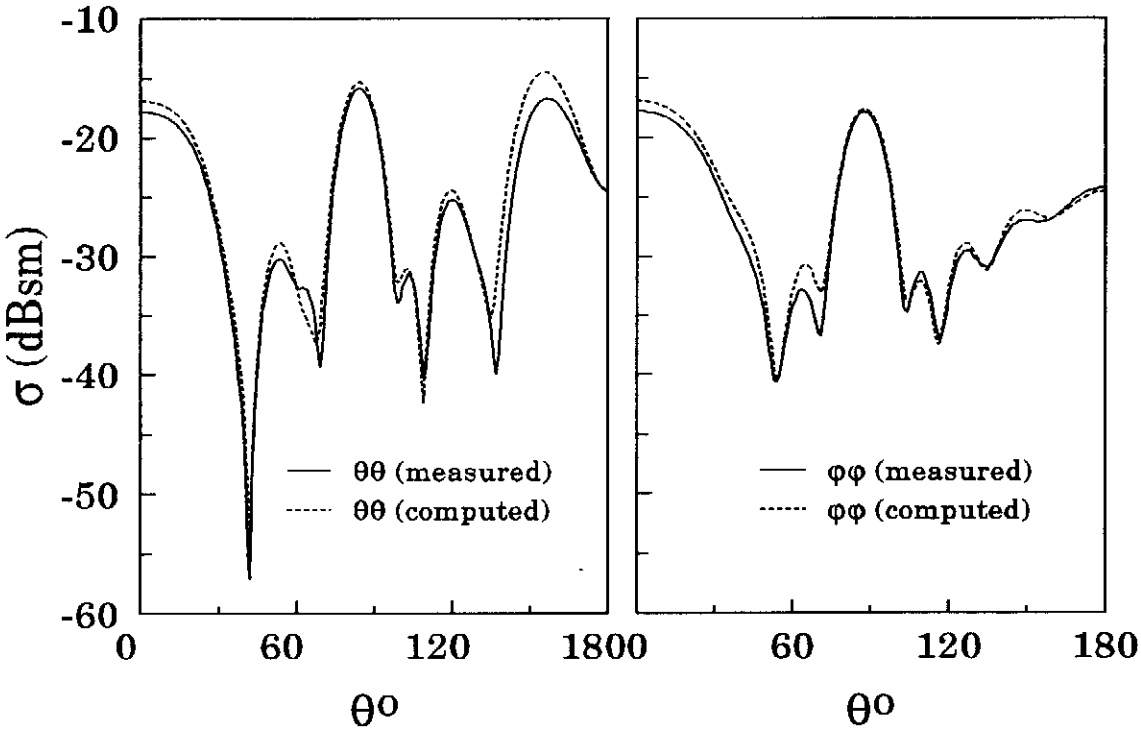

Fig. 13. Computed and measured monostatic RCS of case3 in Fig. 10.

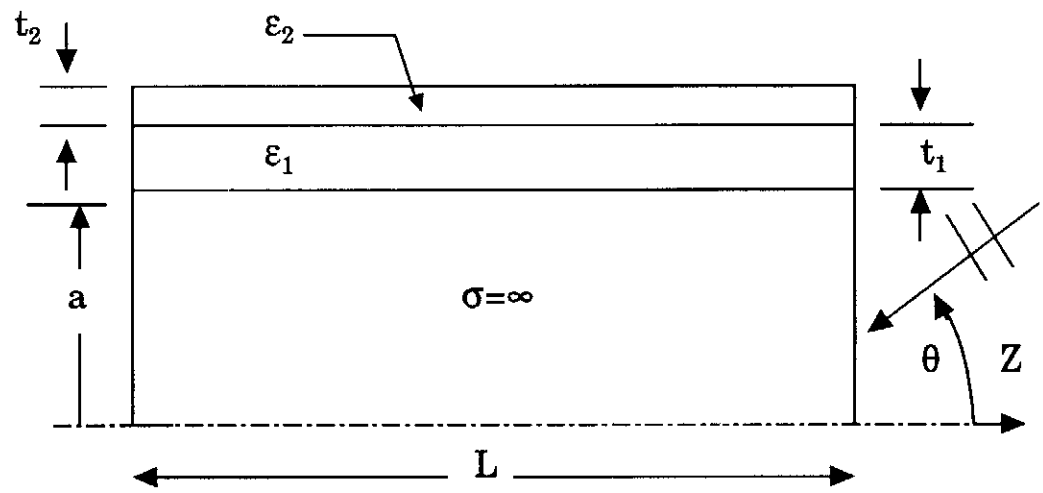

Fig. 14. Geometry of a perfectly-conducting cylinder partially coated with two dielectric layers

Finite cylinders: Another geometry, double layered coating of a finite conducting cylinder, is considered. Figure 14 shows the geometry of the cylinder. The values of the parameters of Fig. 14 are given in Table I for three cases. All the measurements in this section have been performed at 4GHz. Figure 15 (left) shows the comparison between the computed and measured data of the monostatic RCS for $\theta\theta$ polarization of case1 in Table I. In this case only one layer is considered.

Table I. Parameters of Figure 14

case	a(cm)	L(cm)	t_1(cm)	ϵ_{r1}	t_2(cm)	ϵ_{r2}
1	3.0	27.94	0.1528	35.2- j28.68	-	-
2	3.0	27.94	0.1528	35.2-j28.68	0.68	1.757-j1.569
3	2.814	21.59	0.988	2.05	0.1528	35.2-j28.68

The measured data of $\phi\phi$ polarization are not available, however, the computed data are shown in Fig. 15 (right). The monostatic RCS of the second case in Table I of the two layered coating is shown in Fig. 16. Again, only the measurements of the $\theta\theta$ polarization are available. In the last case, the first layer is a high loss material of large permittivity and the second one is high loss of small permittivity. In the third example of Table I, the first layer is made of a lossless material of small permittivity; the second layer is made of high-loss high-permittivity materials. The monostatic RCS is shown in Fig. 17 for the $\theta\theta$ and $\phi\phi$ polarization, respectively. The last three cases represent large objects. The agreement between the measured and computed data is satisfactory. In general, the above results show accuracy of the measurements within a wide dynamic range of sensitivity.

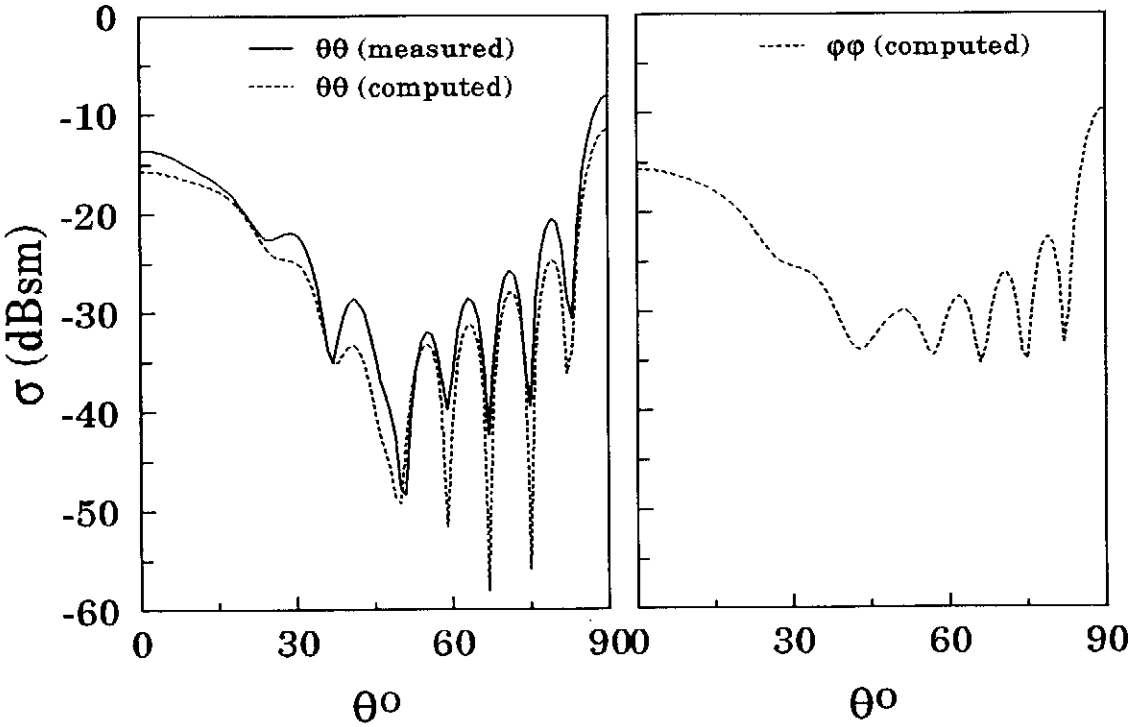

Fig. 15. Computed and measured monostatic RCS of case1 in Table I.

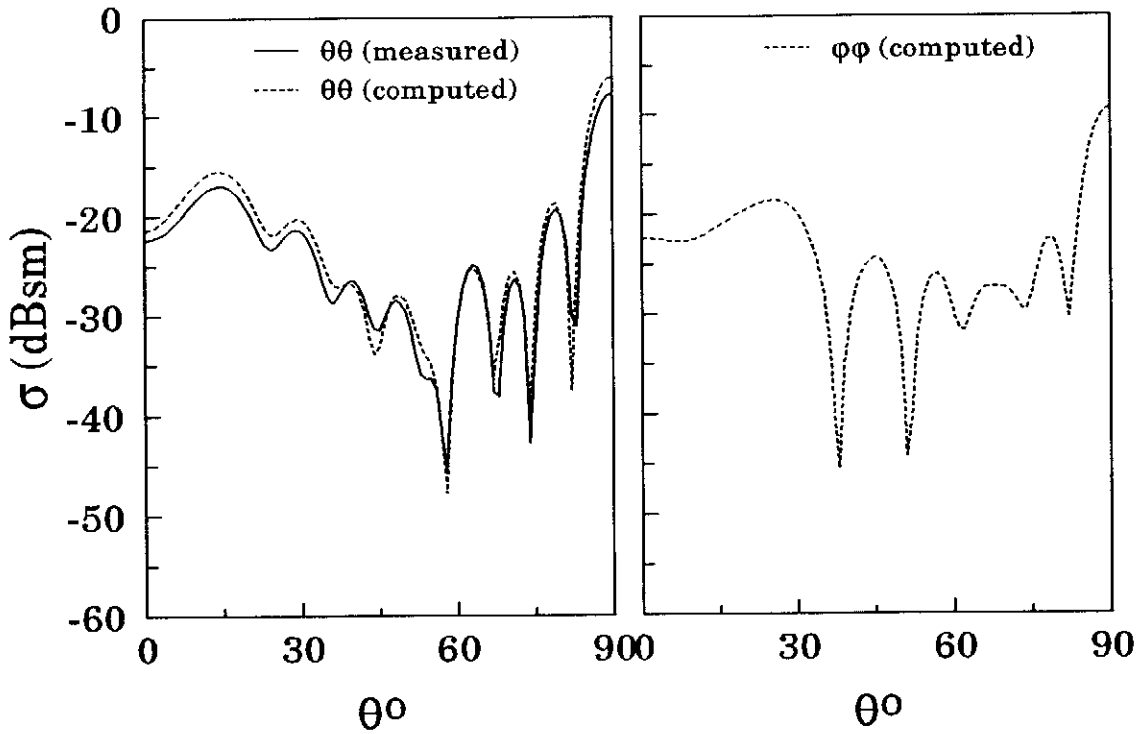

Fig. 16. Computed and measured monostatic RCS of case2 in Table I.

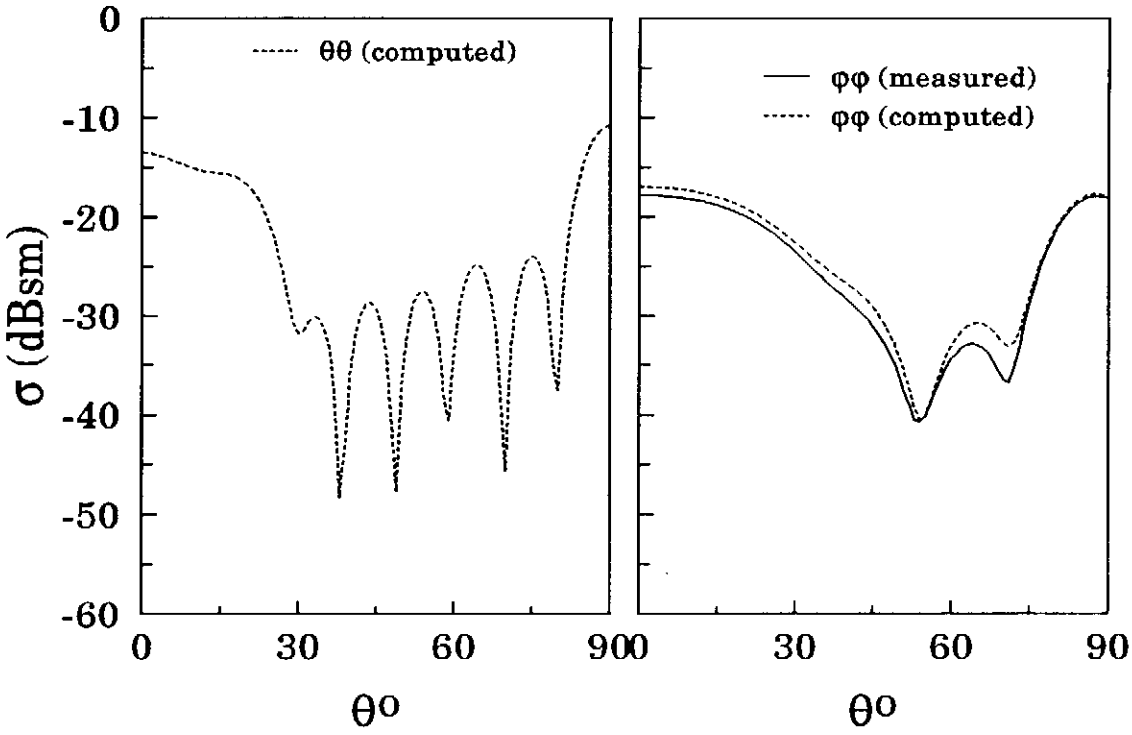

Fig. 17. Computed and measured monostatic RCS of case3 in Table 1.

IV CONCLUSION

In this paper, a computer program has been developed to compute the electromagnetic scattering from axisymmetric objects. The method of moments is used to solve the surface-integral equations formulation (E-PMCHW). A number of objects has been analyzed by this program. Each object consisted of arbitrarily arranged homogeneous regions. Both bistatic and monostatic RCS data were presented. The computed data were verified either numerically or experimentally and excellent agreement was demonstrated.

REFERENCES:

[1] L. N. Medgyesi-Mitschang and J. M. Putnam, "Electromagnetic scattering from axially inhomogeneous bodies of revolution," *IEEE Trans. Antennas Propagat.*, vol. AP-32, p. 797, 1984.

[2] W. Zheng, "The null field approach to electromagnetic scattering from composite objects: The case with three or more constituents", *IEEE Trans. Antennas Propagat.*, vol. AP-36, p. 396, 1988.

[3] S. Storm and W. Zheng, "The null field approach to electromagnetic scattering from composite objects," *IEEE Trans. Antennas Propagat.*, Vol. AP-36, p. 376, 1988.

[4] M. A. Morgan and K. K. Mei, "Finite-element computation of scattering by inhomogeneous penetrable bodies of revolution," *IEEE Trans. Antennas Propagat.*, vol. AP-27, p. 202,1979.

[5] D. -S. Wang and P. W. Barber, "Scattering by inhomogeneous nonspheroidal objects," *Appl. Opt.*, vol. 18, p. 1190, 1979.

[6] A. W. Holt, "The Fredholm integral equation method and comparison with the T-matrix approach, " in *Acoustic, Electromagnetic and Elastic Wave Scattering: Focus on the T-matrix Approach*, V. V. and K. V. Varadan, Eds. London, U. K., Pergamon, p. 255, 1980.

[7] J. R. Mautz and R. F. Harrington, "Electromagnetic coupling to a conducting body of revolution with a homogeneous material region," *Electromagn.*, vol. 2, p. 257, 1982.

[8] J. R. Mautz and R. F. Harrington,"H-field E-field and combined field solutions for conducting bodies of revolution," *Arch. Elektron. Ubertragungstech.* vol. 32, pp. 159-164, 1978.

[9] A. A. Kishk and L. Shafai, "Different formulations for numerical solutions of single or multibodies of revolution with mixed boundary conditions," *IEEE Trans. Antennas Propagat.*, vol. AP-37, p. 666, 1986.

[10] M. Kerker, 'The scattering of light and other electromagnetic radiation', *Academic Press Inc.*, 1969 .